Atomic and electronic structure of few-layer graphene on SiC(0001) studied with scanning tunneling microscopy and spectroscopy

P. Lauffer, K. V. Emtsev, R. Graupner, Th. Seyller,* and L. Ley
Lehrstuhl für Technische Physik, Universität Erlangen-Nürnberg, 91058 Erlangen, Germany

S. A. Reshanov and H. B. Weber
Lehrstuhl für Angewandte Physik, Universität Erlangen-Nürnberg, Germany

(Received 25 November 2007; revised manuscript received 11 February 2008; published 18 April 2008)

Epitaxial growth of graphene on SiC surfaces by solid state graphitization is a promising route for future development of graphene based electronics. In the present work, we have studied the morphology, atomic scale structure, and electronic structure of thin films of few-layer graphene (FLG) on SiC(0001) by scanning tunneling microscopy and spectroscopy (STS). We show that a quantitative evaluation of the roughness induced by the interface is a tool for determining the layer thickness of FLG. We present and interpret thickness dependent tunneling spectra, which can serve as an additional fingerprint for the determination of the layer thickness. By performing spatially resolved STS, we find evidence that the charge distribution in bilayer graphene is inhomogeneous.

DOI: 10.1103/PhysRevB.77.155426 PACS number(s): 68.55.−a, 68.35.−p, 68.37.Ef, 81.05.Uw

I. INTRODUCTION

Graphene, a monolayer of graphite, has recently attracted considerable attention since it was shown that it can be prepared by simple mechanical exfoliation.[1] Subsequent studies of graphene's electronic properties revealed new and interesting physics,[1–6] which arises from graphene's unique electronic band structure. The two bands due to the delocalized π states, i.e., the bonding π band and the antibonding π^* band, are degenerate at the K point of the hexagonal Brillouin zone. In neutral graphene, this crossing point, which is frequently referred to as the Dirac point E_D, lies at the Fermi level and, hence, the Fermi surface is pointlike. Both bands have a linear dispersion in the vicinity of E_D. In addition, the two sublattices are represented by a two-component wave function, which is often interpreted as a pseudospin. As a consequence, the quasiparticle dynamics in graphene is governed by Dirac's equation rather than by Schrödinger's equation. The quasiparticles in graphene thus behave like massless Dirac fermions. Altogether, this leads to unconventional physics, for example, to a novel half-integer quantum Hall effect[2,3,6] that has been observed even at room temperature.[6] It has also been suggested that the unique properties of graphene may open a route toward carbon based nanoelectronics for quantum computing.[3,5,7]

Many of the exciting results in graphene research have been obtained on a material produced by mechanical exfoliation. However, there is also an alternative route for the fabrication of graphene, which is based on the solid state graphitization of silicon carbide (SiC) surfaces[8–12] by annealing SiC at temperatures above 1150 °C. This method has the potential to lead to a reproducible, large scale production of graphene, which is the prerequisite for the development of graphene based electronic devices.[4,5,7]

Graphene and thin films of multilayered graphene, so-called few-layer graphene (FLG), grown on hexagonal SiC surfaces have been characterized by several methods such as transport measurements,[4,5] angle-resolved photoelectron spectroscopy (ARPES),[13–21] x-ray diffraction,[22–24] and scanning tunneling microscopy (STM) and spectroscopy (STS).[25–28] With the exception of scanning tunneling microscopy and spectroscopy, all these methods have a limited lateral resolution and the results show the properties averaged over a large area of the sample. On the other hand, STM and STS provide information on the atomic scale and are therefore complementary to the other methods.

The STM/STS studies published so far have concentrated on different aspects. Mallet *et al.*[25] showed that monolayer and bilayer graphene on SiC(0001) can be distinguished by STM. Graphene shows rings with six protrusions, while bilayer graphene shows only three protrusions like graphite due to symmetry breaking caused by the AB stacking of the individual layers. In addition, they demonstrated that the $(6\sqrt{3}\times 6\sqrt{3})R30°$ reconstructed interface layer ($6\sqrt{3}$ for short) remains visible through the graphene layers when imaged at high bias and that scattering of charge carriers on pointlike defects leads to the appearance of characteristic interference patterns. Rutter *et al.*[26] studied such interference patterns in more detail and discussed scattering mechanisms in monolayer and bilayer graphene. Brar *et al.*[27] performed STS on monolayer and bilayer graphene and found a gap around the Fermi level with unclear origin. A very recent paper from Riedl *et al.*[28] reexamines the atomic structure of the $6\sqrt{3}$ reconstruction and demonstrates that the appearance of that reconstruction in STM is bias dependent. The image therefore contains information about the electronic structure and not just topological information as claimed in another work by Chen *et al.*[29]

In the present work, we first focus on the morphology and structure of FLG films with thicknesses ranging from 1 to 4 ML (monolayer). One of the most pressing questions in STM studies of FLG is the determination of the layer thickness. While this is rather straightforward in ARPES[17] and low-energy electron microscopy,[30,31] the determination of the layer thickness by STM requires great care. We demonstrate that an interface-induced roughness in FLG films on

SiC(0001) can be used to quantitatively gain information about the layer thickness. Using this information, we show that the determination of the layer thickness just by an inspection of the STM image can lead to errors. After establishing a method for the determination of the thickness of our FLG films, we study the electronic structure of these films by STS and show that features in the dI/dV spectra can be explained by the density of states (DOS) of FLG. Thus, we provide an additional fingerprint for the determination of the FLG layer thickness through STM. Finally, the dependence of tunneling spectra on the exact position within the unit cell of the interface structure will be discussed.

II. EXPERIMENT

Graphene and FLG with a thickness of up to 4 ML were grown on nitrogen doped SiC(0001), purchased from SiCrystal, by using solid state graphitization.[8–12] Prior to that, the sample surfaces were etched in hydrogen [$T=1550$ °C; $p_{H_2}=1$ bar, flux of 3 slm (standard liter per minute), and $t=15-20$ min]. The average FLG film thickness was determined by x-ray photoelectron spectroscopy (XPS) using a simple layer attenuation model.[20] The samples were then introduced into the STM chamber where they were degassed overnight at a temperature of 450 °C. XPS and ARPES measurements indicate that this treatment is sufficient to remove surface contaminants from FLG films. Furthermore, using XPS, we have observed that the $6\sqrt{3}$ reconstruction is also stable in air.[35]

STM and STS measurements were carried out using an Omicron LT-STM cooled with liquid nitrogen to $T\approx 80$ K. The tips were fabricated from a Pt-Ir wire by electrochemical etching and subsequently cleaned by Ar ion etching in ultrahigh vacuum. STM images in constant current mode were obtained at tunneling currents of typically 5 pA at a sample bias of $U_T\approx -100$ mV. Scan speed was around 10 nm/s.

Differential conductance spectra were measured directly via a lock-in amplifier. For this purpose, the tunneling bias was modulated with an amplitude between 12 and 16 mV_{rms} at a frequency of 793 Hz. To obtain tunneling spectra, the tip-sample distance was fixed by setting $I_T=250$ pA at $U_T=-0.6$ V. Then the feedback loop was switched off and six subsequent tunneling spectra were recorded in order to guarantee reproducibility. In addition, the STS curves presented here are typically averaged over 14–21 independent spatial points.

III. RESULTS AND DISCUSSION

A. Scanning tunneling microscopy

1. Thickness and roughness of few-layer graphene

In this section, we discuss long-range variations in the image contrast caused by the interface structure. We will show that an evaluation of this phenomenon can serve as a tool to determine the layer thickness of epitaxial graphene films on SiC(0001).

Figures 1(a) and 1(b) show STM images of 1 ML of graphene grown on SiC(0001). Both images were obtained at a large bias voltage of $U_T=-1.85$ V, where no atomic resolution is observed as evident from the image of the smaller area shown in Fig. 1(b). At such high tunneling voltages, the states contributing to the image are not the electronic states of the graphene layer. Instead, the underlying SiC surface is imaged,[25] which is covered by the nonmetallic $6\sqrt{3}$ reconstruction,[19] previously studied by STM.[28,32–34] Despite the fact that the reconstruction has a $6\sqrt{3}$ periodicity,[28,33,34] the periodicity seen in the STM images shown is (6×6), in agreement with previous reports.[25–27,29,32–34] Recently, it was shown that a careful imaging of the clean $6\sqrt{3}$ reconstruction leads to images where the true periodicity is visible.[28] It is evident from the images shown in Fig. 1 that the reconstruction is not perfectly regular but spreads somewhat in a lateral position and an apparent height, again in agreement with the previous studies.[25–28,33,34] Other than that, the surface appears to be flat and homogeneous even in the large scale image shown in Fig. 1(a). Note that the contrast due to the $6\sqrt{3}$ reconstruction does not change in that image. According to the discussion below, this indicates that the thickness of the graphene layer covering the $6\sqrt{3}$ reconstructed interface is constant over an area of 60×60 nm^2. We routinely achieved areas of 100×100 nm^2 in size covered by the same graphene thickness.

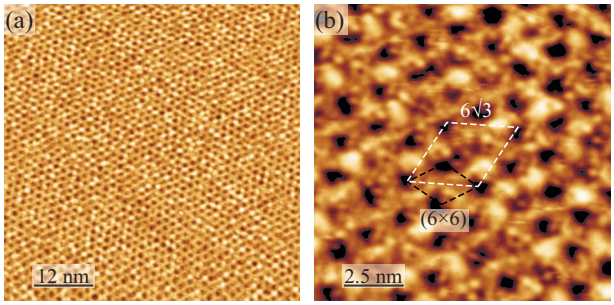

FIG. 1. (Color online) STM images of SiC(0001) covered with 1 ML graphene taken at a large bias voltage of $U_T=-1.85$ V ($I_T=7$ pA). The z scale is 0.00–0.866 Å in (a) and 0.00–0.83 Å in (b).

For a closer inspection of the graphene lattice, we decreased the scale and the bias voltage. Figure 2(a) shows an area where we did not succeed in decreasing the bias to values below $U_T=-0.54$ V. From a comparison with literature,[25,33,34] we conclude that this image shows an area covered by the $6\sqrt{3}$ reconstruction. It is clear from Fig. 2(a) that there is a large corrugation, which agrees with previous reports,[25] and also some lateral disorder. Individual atoms were only recently imaged by the group of Riedl *et al.*[28] and we refer the reader to the discussion of the structure in that work. Note, however, that despite the apparent disorder, the $6\sqrt{3}$ reconstruction has a very well developed electronic dispersion relation.[19]

Figure 2(b) shows the atomically resolved image of 1 ML of graphene imaged at $U_T=-114$ mV ($I_T=5$ pA). Atomic resolution of the graphene lattice was observed to appear at sample biases below −200 mV. Clearly, two independent periodicities are visible: the apparent (6×6) periodicity of the $6\sqrt{3}$-reconstructed SiC(0001) surface and the honeycomb lattice of graphene. As already seen in Fig. 1, the height variation due to the interface layer is not perfectly regular. On the

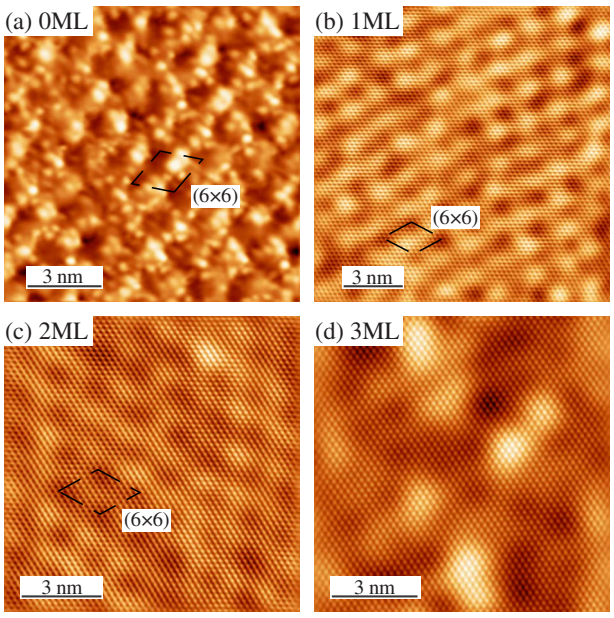

FIG. 2. (Color online) STM images of FLG films with well-defined thicknesses. (a) 0 ML (U_T=−540 mV, I_T=8 pA); z scale is 0–191 pm. (b) 1 ML (U_T=−114 mV, I_T=7 pA); z scale is 0–96 pm. (c) 2 ML (U_T=−0.114 mV, I_T=5 pA); z scale is 0–78 pm. (d) 3 ML (U_T=−110 mV, I_T=5 pA); z scale is 0–28 pm. The roughness caused by the interface layer decreases with increasing layer thickness (see text).

other hand, the graphene layer on top is perfectly ordered. No atomic defects (defects of type B in Ref. 26) are present in the image although such defects were observed occasionally.

Bilayer graphene is shown in Fig. 2(c). It is obvious that the interface-induced corrugation is reduced as compared to the monolayer case. At the same time, the atomic corrugation due to the graphene lattice is enhanced. Figure 2(d) shows a STM image obtained with 3 ML graphene. The height variation ascribed to the interface layer has become even less pronounced (note the different z scales of the images) and, at the same time, appears to become somewhat more irregular. The bright (high) areas in the image may well be equivalent to the type A defects (mounds) in Ref. 26. The graphite lattice on top is perfectly periodic and, again, there is no evidence of atomic scale defects (type B in Rutter's notation) in that image.

A more quantitative analysis of the interface layer induced height variations in the STM images was performed using a quantity that we call the interface-induced roughness R. R is the rms roughness of the surface determined after convolution of the STM image with a Gaussian with a width corresponding to the graphene lattice parameter. This treatment smoothes away contributions to the roughness by the graphene lattice. The remaining height variations are then mainly due to the roughness induced by the interface layer. The result is shown in Fig. 3. It is obvious that the interface-induced height variations decrease monotonically with layer thickness. The dashed line in Fig. 3 is the result of a fit using a simple exponential decay $R=R_0+Ae^{-t/\lambda}$. The fit yields a nonvanishing terminal roughness R_0 of 5 ± 2 pm, which is

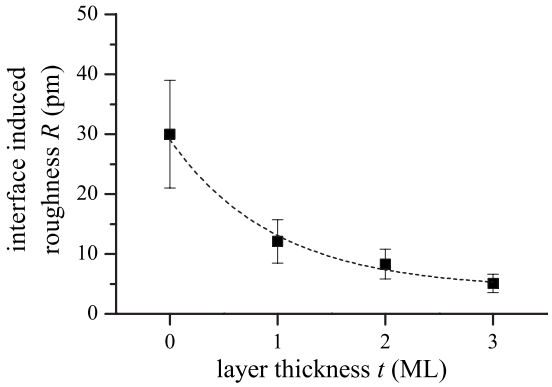

FIG. 3. Interface-induced roughness R as a function of layer thickness t in ML. For explanation, see text.

caused by any long-range disorder such as, e.g., the mounds mentioned above. The decay constant λ amounts to 0.8 ± 0.2 ML, which corresponds to 0.27 ± 0.07 nm, if we assume that the layer distance is that of graphite (0.335 nm). The error bars in Fig. 3 are mainly caused by variations in the tip geometry. A further contribution stems from variations in the tunneling set points. For example, for monolayer graphene, we observed that the interface layer roughness decreases by approximately 20% from 12.1 to 10 pm when going from U_T=−100 mV to U_T=−430 mV, but remains fairly constant between U_T=−430 mV and U_T=−1.8 V. Similar observations were reported by other groups,[25–27] but not systematically quantified to the same extent as shown here. Brar *et al.*[27] determined rms roughnesses of 20 and 10 pm at V_T=1.0 V for monolayer and bilayer graphene on SiC(0001), respectively. In agreement with our observations, there is a decrease in the roughness with growing layer thickness. Their numerical values, however, include also contributions due to the atomic structure of the graphene lattice, which are not included in our analysis. It is thus no surprise that the roughness values reported by Brar *et al.*[27] are somewhat larger than our results. Second, as already mentioned above, the exact numerical values also vary from tip to tip. Keeping this in mind, we find a rather good agreement between our study and the work of Brar *et al.*[27] In any case, the interface-induced roughness as introduced in the present work is a useful means to determine the layer thickness as will be shown below.

2. Stacking in few-layer graphene

We now turn our attention to the image contrast caused by the graphene lattice itself and investigate its dependence on the layer thickness. Figure 4 shows close-up images revealing the variation of the atomic structure of the FLG films with different thicknesses. The image of a monolayer graphene is given in Fig. 4(a). It shows smeared-out hexagons. One of these hexagons is highlighted to guide the eye. Such an observation is, indeed, expected for graphene, where the two atoms per unit cell are equivalent and should lead to a symmetric appearance in STM. The observation also agrees well with previous reports of graphene on SiC(0001) (Refs. 25 and 27) and exfoliated graphene on SiO_2.[36]

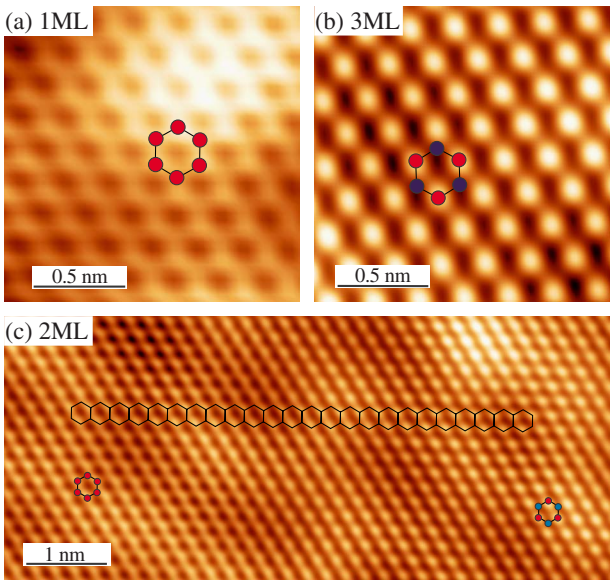

FIG. 4. (Color online) (a) Atomically resolved structure of 1 ML graphene imaged at $U_T=-114$ mV and $I_T=7$ pA (z scale is 0–82 pm). (b) 3 ML graphene imaged at $U_T=-110$ mV and $I_T=5$ pA (z scale is 0–10 pm). (c) Bilayer graphene imaged at $U_T=-0.114$ mV, $I_T=5$ pA (z scale is 0–75 pm). The honeycomb structure of graphene is indicated by hexagons showing equivalent atoms for a monolayer case and inequivalent atoms for the trilayer case and part of the bilayer case.

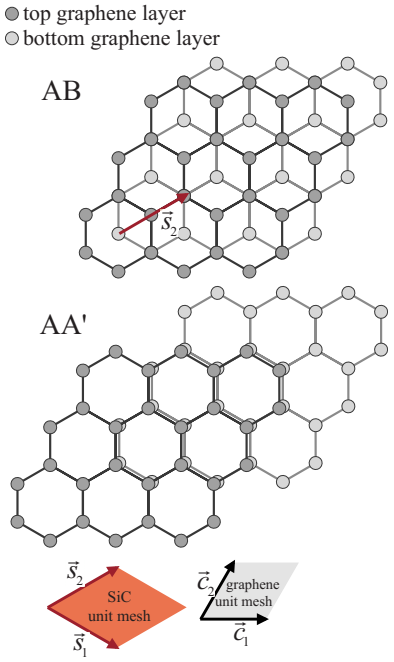

FIG. 5. (Color online) Creation of an AB/AA' transition. The bilayer in the top graph follows the natural AB stacking. Shifting the bottom layer by the SiC surface unit vector $\vec{s}_2$ results in a stacking close to an AA configuration (therefore AA') as shown in the bilayer on the left hand side. The STM image of such a configuration is expected to look more like that of a graphene monolayer.

Figure 4(b) shows the atomically resolved image of 3 ML graphene on SiC(0001). The substructure strongly differs from the monolayer case. Only one out of two atoms is seen by STM. For the hexagon, this means that only three out of six atoms lead to protrusions, which is frequently called the three-for-six arrangement. This observation is in agreement with STM measurements on highly ordered pyrolytic graphite and can be explained by the fact that the AB stacking of the layers in graphite breaks the symmetry, leading to two inequivalent C atoms per unit cell.[25,27,36]

Figure 4(c) was observed on bilayer graphene. On the right hand side, the image shows a triangular array of bright spots similar to the 3 ML case. This is expected for a bilayer with AB stacking.[25,27,36] In fact, most of the atomically resolved images of bilayer graphene (see also below) show such an arrangement. The image of Fig. 4(c), however, is of particular interest because on the left hand side, the image resembles that of a graphene monolayer. Note that there is no step visible in this image and that the interface-induced roughness is the same on both sides of the image. Therefore, we can safely state that we image the same layer thickness in both parts of the image. As a possible explanation of this observation, we propose that there is a change of stacking underneath the top layer. Whereas the underlying graphene layer follows AB stacking in the right part of the image, it is shifted away from the AB registry in the left part of the image. As shown in Fig. 5, a configuration AA' close to AA stacking is obtained when the bottom layer of the bilayer system is shifted by a SiC basal plane unit vector. The AA' stacking should have a similar contrast as the AA stacking and could therefore account for the observed image. Such an observation demonstrates, however, that an identification of the layer thickness based exclusively on the contrast of the graphene lattice (hexagons vs triangular) could lead to errors.

3. Growth of few-layer graphene

The atomically resolved image in Fig. 6(a) contains a step of the SiC substrate. The graphene lattice is clearly imaged on both the upper and the lower terrace [Figs. 6(c) and 6(d)], with the lattice orientation remaining unchanged. In fact, the graphene lattice is not interrupted by the step, as is clearly evident from the three-dimensional (3D) representation displayed in Fig. 6(b). This is in agreement with earlier reports for the growth of thicker graphitic layers on 8° off-axis oriented 4H-SiC(0001),[13,37] where a carpetlike growth mode covering several substrate terraces and steps was observed. The relation between the FLG lattice and the SiC(0001) substrate lattice allows us to identify that the step runs parallel to the $[11\bar{2}0]$ direction of the SiC substrate just as the steps observed for our hydrogen etched, nominally on-axis oriented SiC(0001) substrates before graphene growth (not shown).

In order to determine the layer thickness, we have determined the interface-induced roughness as discussed above and obtain $R=7.9\pm0.8$ pm and $R=13.0\pm1.0$ pm for the lower terrace and upper terrace, respectively. A comparison with the data shown in Fig. 3 allows us to conclude that the layer thickness is 1 ML on the upper terrace and 2 ML on the lower terrace. This is in agreement with the STM image of the lower terrace in Fig. 6(d), which shows a three-for-six

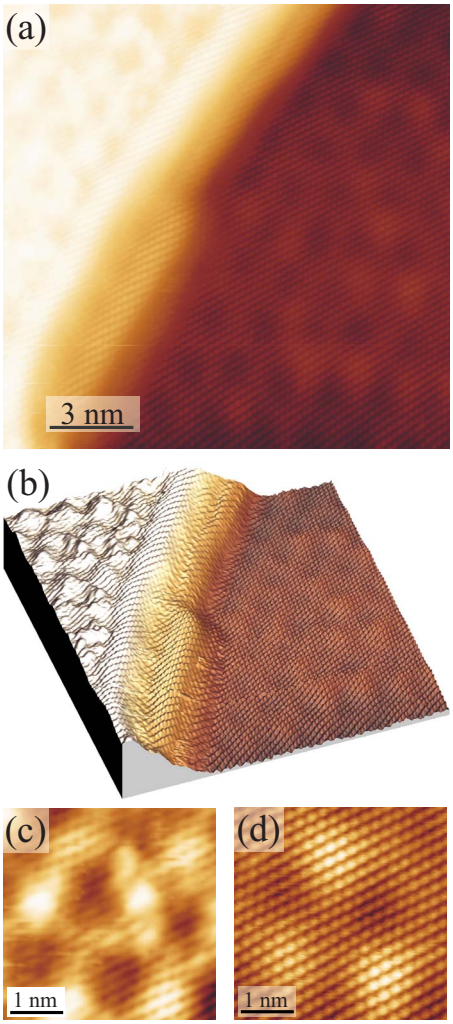

FIG. 6. (Color online) (a) Atomically resolved STM image of a graphene-covered SiC step imaged at U_T=−0.159 mV and I_T =5 pA. The z scale is 0–0.52 nm. (b) 3D visualization of the image shown in (a). (c) Close-up of the upper terrace. (d) Close-up of the lower terrace.

appearance caused by *AB* symmetry breaking. The image of the upper terrace in Fig. 6 is not as clear. However, instead of individual protrusions like on the lower terrace, the upper terrace shows dark spots surrounded by bright areas. The deviation from a hexagonal shape might be due to the presence of the step, which may cause some uniaxial strain. The identification of the layer thickness on the upper and lower terraces is further supported by STS, as shown below.

It is interesting to analyze the step height. For that purpose, the height distribution of the image in Fig. 6(a) was determined. The result is shown in Fig. 7. The histogram exhibits three distinct maxima. The large maximum at a height of 0.05 nm is due to the lower terrace and the second maximum at 0.45 nm is caused by the upper terrace. Thus, the step height is 0.40 nm, which does not fit the interlayer spacing of graphite (0.335 nm). A further maximum in the height distribution at 0.29 nm, i.e., 0.24 nm above the lower graphene terrace, is close to the SiC bilayer spacing (0.252 nm). This maximum in the height distribution corresponds to the narrow terrace located at the side of the step.

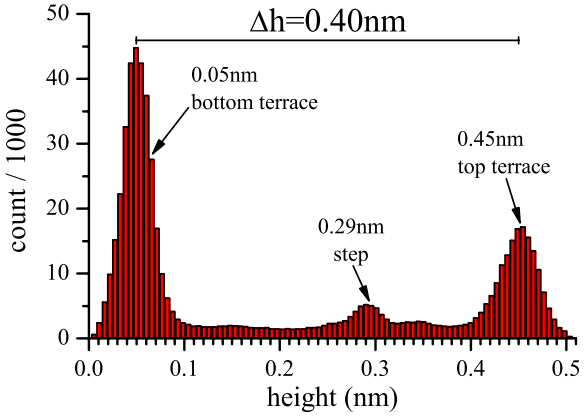

FIG. 7. (Color online) Height distribution of the image shown in Fig. 6(a). The left and the right maxima correspond to the lower and upper terraces of the step, respectively. The step height is Δh =0.40 nm. The small maximum corresponds to the small terrace on the side of the step in the lower half of the image in Fig. 6(a).

In order to explain the step height of 0.40 nm, we consider a SiC(0001) surface covered by the $6\sqrt{3}$ reconstruction, which is the precursor to graphene growth on SiC(0001) and a single graphene layer, as shown on the left of Fig. 8. If we now grow an additional layer in the right half of Fig. 8 by thermal evaporation of Si, we have to consume SiC material. The area density of C atoms in graphene (3.82×10^{15} cm^{-2}) is about three times that of C atoms in a SiC bilayer (1.22×10^{15} cm^{-2}). Thus, the growth of one graphene layer consumes three layers of SiC as indicated in Fig. 8. Accordingly, the expected height difference is the difference between three times the SiC interlayer spacing and the graphite interlayer spacing: Δh=0.421 nm. Note that the unknown quantities x and d_{01} in Fig. 8 cancel. This value agrees to within 5% with the measured step height of 0.40 nm.

The step observed here can thus be explained by considering an initially flat terrace. After the growth of 1 ML graphene on the whole terrace, an additional layer has formed on only a part of the terrace. The fact that the step is continuously covered suggests that the second layer grows underneath the first layer by out-diffusion of Si. This picture is supported by the observations on bilayer graphene discussed above, where a change of stacking underneath the top layer was proposed in order to account for the different image contrast of bilayer graphene. Obviously, such a situation comes as no surprise when the growth of graphene occurs underneath and not on top of the existing layers.

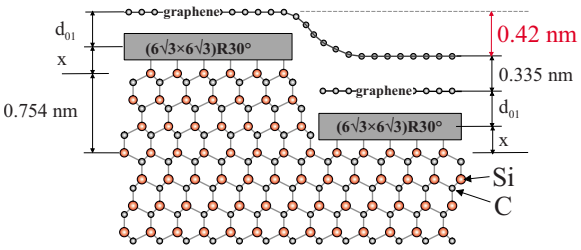

FIG. 8. (Color online) Explanation of the step height observed in Fig. 6(a) and quantified in Fig. 7. For details, see text.

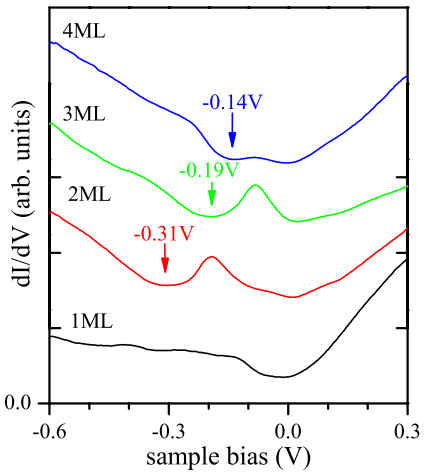

FIG. 9. (Color online) Representative dI/dV spectra of FLG with different thicknesses. For clarity, the spectra are vertically offset from each other and their zeros indicated by tick marks.

B. Scanning tunneling spectroscopy

In this section, we concentrate on results from STS. In particular, we discuss how the tunneling spectra depend on the thickness of the layer and how they can be interpreted in terms of the DOS of FLG calculated by a tight binding model.

Figure 9 displays representative dI/dV curves of FLG layers with different thicknesses. The spectra shown in that figure are averages of spectra taken over several points (between 11 and 21) along lines connecting topological minima or maxima caused by the interface layer (see also the discussion below), i.e., they cover several graphene unit cells lying above different positions of the $6\sqrt{3}$ interface structure. Common to all dI/dV spectra is a minimum at zero bias but without reaching zero. A similar study of graphene on SiC(0001) by Rutter *et al.*[26] also shows a local minimum at zero bias. In that case, dI/dV remains finite, too. In contrast, Brar *et al.*[27] found a minimum for both monolayer and bilayer graphene, where the dI/dV curve drops down to zero. This was interpreted as a gap in the electronic structure and its origin was discussed. However, a definitive explanation of this observation cannot be provided at present.

In addition to the zero bias minimum, the dI/dV spectra of 2, 3, and 4 ML graphene are characterized by local minima at negative biases followed by a pronounced maximum. Both shift steadily toward zero bias with increasing thickness (see Fig. 9). The minima at −0.31, −0.19, and −0.13 V, respectively, fit well to the position of the Dirac point E_D as observed by ARPES.[14,16,17,21] We therefore propose that these minima mark the position of the Dirac point in our FLG films.

Before we turn our attention to the interpretation of the experimental dI/dV curves of multilayer graphene, we shall discuss some more the spectrum of monolayer graphene. For graphene, a linear DOS with a minimum at $E_D = (0.48 \pm 0.05)$ eV below E_F (Refs. 14, 16, 17, and 21) is expected. The measured tunneling spectrum shown in Fig. 9 and also the data of Brar *et al.*[27] do not agree with that expectation. Note also that no gap is observed at the Dirac energy, which was suggested by Zhou *et al.*[21] to have a magnitude of 260 mV. However, the interpretation of tunneling spectra of monolayer graphene on SiC(0001) in terms of the graphene band structure is difficult because of the underlying $6\sqrt{3}$ interface layer, which can contribute to the tunneling current.[25] This $6\sqrt{3}$ interface layer has been studied by ARPES,[19,20] and a weakly dispersing state was observed at (0.5 ± 0.1) eV, i.e., at the same energy where E_D is expected for the monolayer graphene sample. The contribution of the interface layer to the tunneling current is expected to exponentially decay with the thickness of the FLG layer so that the undistorted electronic structure of the films will become observable for multilayers, as will be demonstrated below.

In order to interpret the spectra in terms of the band structure of bi-, tri-, and quadlayer films, we have calculated the DOS for different thicknesses by using the generalized tight binding (TB) Hamiltonian[17,38–40]

$$\mathcal{H} = \begin{pmatrix} \alpha_1 & \beta_0 & & & & \\ \beta_0^{\mathrm{T}} & \alpha_2 & \beta_s & & & \\ & \beta_s^{\mathrm{T}} & \alpha_3 & \beta_0 & & \\ & & \beta_0^{\mathrm{T}} & \alpha_4 & \beta_s & \\ & & & \beta_s^{\mathrm{T}} & \ddots & \\ & & & & & \alpha_{\mathrm{N}} \end{pmatrix},$$

$$\alpha_i = \begin{pmatrix} E_i & v\pi^{\dagger} \\ v\pi & E_i \end{pmatrix}, \quad \beta_s = \gamma_1 \begin{pmatrix} 0 & s \\ 1-s & 0 \end{pmatrix},$$

where E_i is the on-site Coulomb energy for layer i, $\pi = p_x + ip_y$, γ_1 is the interlayer hopping integral, and v is the band velocity. The on-site Coulomb potential is caused by a layer dependent charge density as discussed in detail elsewhere.[14,17] Different stacking orders are dealt with by the variable s, which is 0 for Bernal $(ABA\ldots)$ and 1 for rhombohedral $(ABC\ldots)$ stacking.[17] The reference energy is the Fermi level E_F, and $E_D = \mathrm{Tr}(\mathcal{H}/2N)$. N is the number of layers. The parameters used in the calculations were initially taken from Ref. 17 and then optimized for agreement between experimental dI/dV spectra and calculated DOS. The values are compiled in Table I. Note that the model Hamiltonian used here neglects the effect of trigonal warping.

Figures 10(a)–10(c) show a comparison of measured dI/dV spectra from 2, 3, and 4 ML thick FLG films with the calculated DOS. For clarity, the tight binding band structure is also shown for $\vec{k}_{\parallel}$ values in the range of ± 0.15 Å^{-1} around the K point in such a way that the energy scale coincides with the scale of the bias voltage. Since trigonal warping is neglected, the band structure is symmetric around the K point, which is, strictly speaking, only valid at energies close to E_D.

The case of bilayer graphene is depicted in Fig. 10(a). Three different measurements (two on different areas of the same sample and one from a different sample) are shown (black lines) together with the calculated DOS (red solid line). The DOS shows two singularities at −0.36 and −0.24 V, which are due to the top of the upper π band and the bottom of the lower π^* band, respectively. In addition, a

TABLE I. TB parameters to reproduce measured dI/dV spectra for $N=2-4$ layers graphene. The errors in the potentials E_i are around ± 0.02 eV. Also shown are the parameters of Ohta *et al.* (Ref. 17).

N	v (10^6 m/s)	E_D (eV)	E_1 (eV)	E_2 (eV)	E_3 (eV)	E_4 (eV)	γ_1
			Present work				
2	1.06	−0.30	−0.36	−0.24			0.46
3	1.06	−0.22	−0.34	−0.16	−0.14		0.44
4	1.05	−0.11	−0.28	−0.10	−0.03	−0.01	0.44
			Ref. 17				
2	1.05	−0.30	−0.35	−0.24			0.48
3	1.06	−0.21	−0.34	−0.16	−0.14		0.44
4	1.06	−0.15	−0.37	−0.10	−0.06	−0.05	0.44

steplike feature is observed in the DOS at 0.16 eV. This is due to the bottom of the upper π^* band. The lower π band is not seen in this energy range. In order to account for broadening effects due to the lifetime of the quasiparticles as well as inhomogeneous broadening, the DOS was convoluted with a Gaussian of width $\omega_G=0.2$ eV. The broadened DOS is also shown in Fig. 10(a) as dashed red lines. The broadening results in a filling of the gap and a smoothing of the singularities, which shifts their maxima away from the gap. In addition, it smears out the steplike feature caused by the upper π^* band. Comparing the broadened DOS with the experimental spectra reveals that the main features of the dI/dV spectrum are well reproduced. This holds, for example, for the minimum at −0.3 eV and the peak at −0.19 eV. The singularity at −0.36 eV, shifted to −0.40 eV, is also apparent as a shoulder in dI/dV (see arrow). The inflection point in the DOS due to the bottom of the second π^* band is also reproduced well after broadening at +0.13 eV (see arrow).

Figure 10(b) displays the spectra obtained for trilayer graphene together with a calculated DOS before and after broadening. A level of agreement comparable to the 2 ML case is achieved. In particular, the gap and the two flanking singularities in the DOS are well reproduced by the various spectra, especially the one labeled C2. Interestingly, in order to obtain this agreement, we had to assume rhombohedral *ABC* stacking. Bernal *ABA* stacking does not reproduce the features of the experimental curves. The presence of rhombohedral *ABC* stacking has recently been derived from ARPES measurements.[17] There, a coexistence of *ABA* and *ABC* stacking was observed, which is reasonable because ARPES averages a large area (typically $\geqslant 100\ \mu m^2$). Note that the total energy difference between *ABA* and *ABC* stacked trilayer graphene is very small (0.18 meV/atom),[41] so that the presence of both configurations is not surprising. STM is a local probe and we cannot exclude that Bernal *ABA* stacking is present in other regions of the sample. Finally, Fig. 10(c) compares the experimental tunneling spectra obtained for 4 ML graphene on SiC(0001) with the calculated DOS for *ABAB* stacking. Again, most features of the tunneling spectra are reproduced by the simulation. Assuming different stacking sequences (e.g., ABCA) leads to worse agreement.

As discussed above, the corrugation of the $6\sqrt{3}$ reconstruction at the interface causes a roughness in the STM images of FLG taken at low biases, which declines with increasing layer thickness. Therefore, we have generally measured STS spectra on equally spaced points along lines that pass through the centers of neighboring rings derived from the $6\sqrt{3}$ reconstruction of the interface. The spectra shown in Figs. 9 and 10 are averaged over all points along these lines. Now we want to demonstrate that the position with respect to the interface structure has an influence on the tunneling spectra.

Figure 11 shows 21 spectra of bilayer graphene in the form of false color plots, which were taken on points separated by 0.13 nm on a straight line that passes through the centers of two adjacent minima of the interface-induced height variation. It is evident from that figure that the tunneling spectra are quite insensitive to the exact location, especially at a bias voltage of around −110 mV, where most of the atomically resolved images were taken. Besides the good overall agreement between the individual spectra, we notice, however, that the width of the gap around the Dirac point E_D at $V_T=-0.32$ eV varies with position. The gap appears to be somewhat wider at the bottom of the depression caused by the interface structure as indicated by the horizontal arrows in Fig. 11 at positions ~0.2 and ~2.0 nm, respectively, whereas it appears narrower in between at ~1.2 nm, a position that corresponds to the rim. From the data shown in Fig. 11, we estimate a difference in the gap of $\Delta E_g=0.025$ eV. In the tight binding model discussed above, the magnitude of the energy gap is given by the difference in the on-site Coulomb potential $E_g=|E_2-E_1|$. We note in Fig. 11 that the variation of the gap seems to be only on the lower energy side. In our tight binding model, this is equivalent to a local variation of the on-site Coulomb potential E_1 of the layer closest to the substrate such that it is reduced by 25 meV in magnitude at the rim. This change is most likely caused by an inhomogeneous distribution of charge in the graphene layer closest to the substrate, which, in turn, could be induced by the underlying $6\sqrt{3}$ interface structure. Note that the observed spatial variation is very small compared to the overall structure in the spectra so that the interpretation of the spectra in terms of the DOS is still valid.

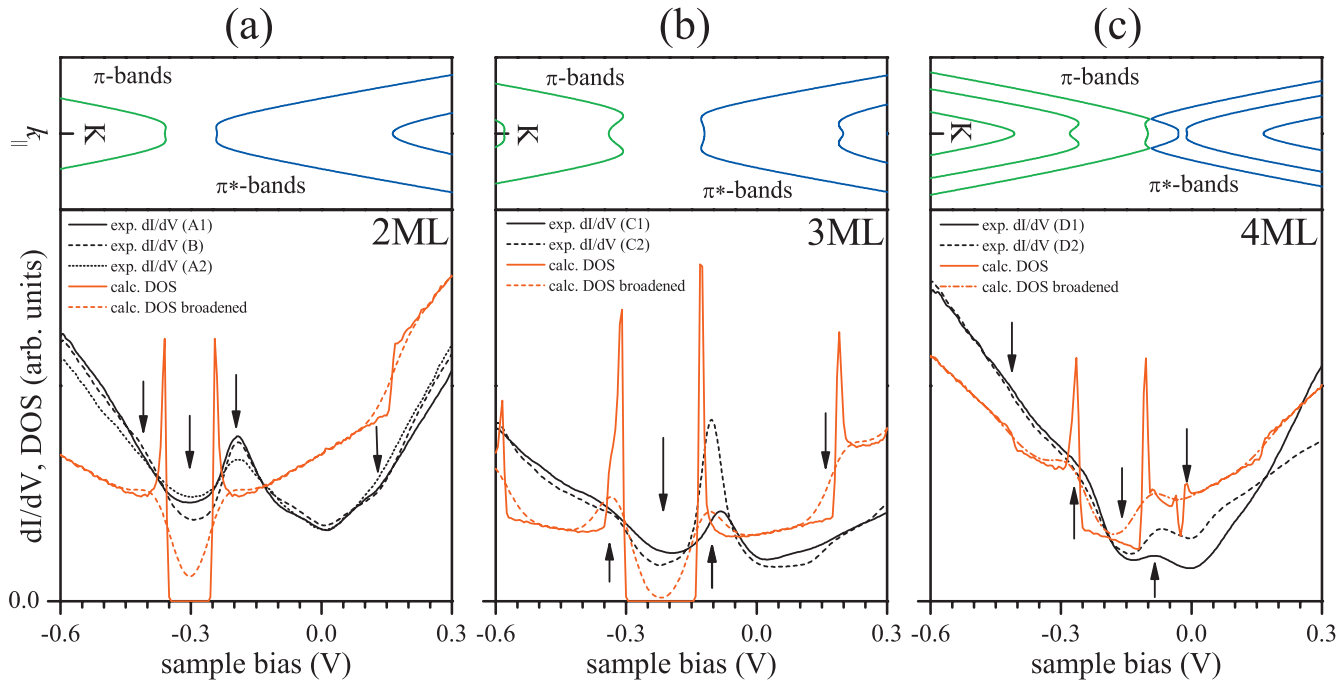

FIG. 10. (Color) (a) Experimental dI/dV curves (black) of FLG films with 2 ML thickness together with the calculated DOS (red) before (solid) and after (dashed) Gaussian broadening with ω_G=0.2 eV. The top panel shows the details of the band structure at the K point. [(b) and (c)] Same as (a) for d=3 and 4 ML, respectively. For details about the calculation, see text. Corresponding features in the broadened DOS and experimental dI/dV spectra are marked by arrows.

IV. CONCLUSION

In the present work, we have used STM and STS at a temperature of 80 K to study the atomic and electronic structures of FLG films on SiC(0001). The FLG films grown on SiC(0001) are situated on top of the $6\sqrt{3}$ reconstruction, which induces long-periodic height variations. The latter are visible in the STM images in addition to the corrugation caused by the graphene lattice. The interface-induced roughness exponentially decreases with FLG thickness in a reproducible way, which has been used to quantify the number of layers. In atomically resolved images, monolayer graphene appears as hexagons and multilayer graphene as a triangular array of protrusions, in agreement with previous reports.[25–27] However, we have also observed areas of bilayer graphene where the image does not show the expected triangular array of protrusions. Unexpectedly, these areas rather resemble the monolayer case. As a possible explanation, we propose a change of stacking underneath the top layer. Thus, the identification of the layer thickness (monolayer vs multilayer) based exclusively on the appearance of the STM image alone is inadequate. As an additional tool, we propose to use the thickness dependence of the interface-induced roughness as quantified here.

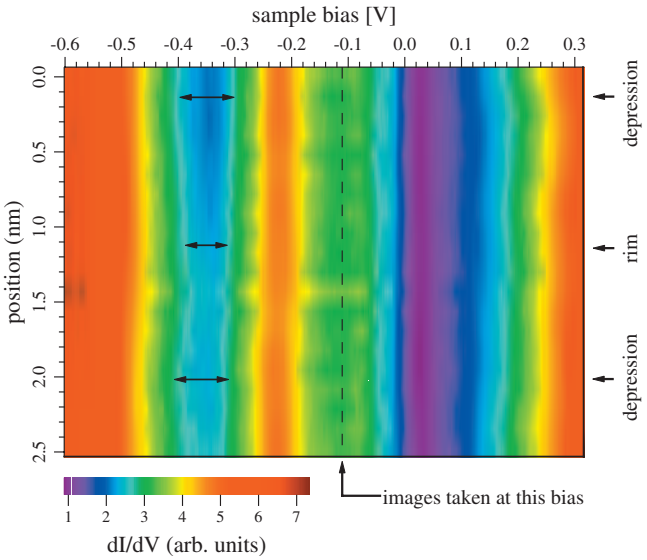

FIG. 11. (Color) Spatially resolved STS spectra of 2 ML graphene on SiC(0001) in a color scale image. The positions corresponding to minima in the interface-induced height variation and to the maximum in between are indicated by arrows on the right hand side and are labeled depression and rim, respectively. The vertical dashed line indicates the bias voltage at which atomically resolved images were taken.

Steps in the SiC substrate were observed by STM, which were covered by FLG without interrupting the graphene structure or any sign of defects. The observation sheds a different light on the growth mechanism of FLG on SiC(0001) in that it strongly supports a scenario where new graphene layers are formed below rather than above the already existing ones.

STS on monolayer graphene was observed to show little agreement with results obtained using ARPES.[14,16,17,21] We propose that the tunneling from the underlying $6\sqrt{3}$ interface layer, which was observed to have occupied states in the energy range around the Dirac point E_D of monolayer graphene,[19,20] obscures the tunneling spectra. A full interpre-

tation of this part of the spectrum in terms of the graphene band structure similar to the multilayer case thus could not be achieved. Clearly, more work is required to fully understand the tunneling spectrum of monolayer graphene on SiC(0001).

The tunneling spectra of FLG show local minima at energies close to those of the Dirac point observed by ARPES.[14,16,17,21] We achieve a close match between structures in the tunneling spectra and the density of states calculated for 2, 3, and 4 ML graphene by using a simple tight binding approach. The spectra thus serve as additional fingerprints for the thickness of the graphene layers. A comparison of tunneling spectra of bilayer graphene obtained above different loci of the interface structure reveals a slight dependence of the band gap energy on the position. The variation of the band gap is consistent with a spatial variation in the on-site Coulomb potential E_1 of the layer closest to the substrate, indicating an inhomogeneous charge transfer. The latter should be caused by local variations of the potential of the $6\sqrt{3}$ interface structure. We propose that this inhomogeneous potential and charge distribution could have an influence on the transport properties of epitaxial graphene and FLG on SiC(0001).

ACKNOWLEDGMENTS

This work was supported by the Deutsche Forschungsgemeinschaft under Contract No. SE 1087/5-1 and WE 3542/5-1. The authors thank M. A. Schneider, T. Ohta, A. Bostwick, E. Rotenberg, and K. Horn for fruitful and stimulating discussions.

*Corresponding author. thomas.seyller@physik.uni-erlangen.de; URL: http://www.tp2.uni-erlangen.de

[1] K. S. Novoselov, A. K. Geim, S. V. Morozov, D. Jiang, Y. Zhang, S. V. Dubonos, I. V. Grigorieva, and A. A. Firsov, Science **306**, 666 (2004).
[2] K. S. Novoselov, A. K. Geim, S. V. Morozov, D. Jiang, M. I. Katsnelson, I. V. Grigorieva, S. V. Dubonos, and A. A. Firsov, Nature (London) **438**, 197 (2005).
[3] Y. Zhang, Y.-W. Tan, H. L. Stormer, and P. Kim, Nature (London) **438**, 201 (2005).
[4] C. Berger *et al.*, J. Phys. Chem. B **108**, 19912 (2004).
[5] C. Berger *et al.*, Science **312**, 1191 (2006).
[6] K. S. Novoselov, Z. Jiang, Y. Zhang, S. V. Morozov, H. L. Stormer, U. Zeitler, J. C. Maan, G. S. Boebinger, P. Kim, and A. K. Geim, Science **315**, 1379 (2007).
[7] A. K. Geim and K. S. Novolselov, Nat. Mater. **6**, 183 (2007).
[8] A. J. Van Bommel, J. E. Crombeen, and A. Van Tooren, Surf. Sci. **48**, 463 (1975).
[9] L. I. Johansson, F. Owman, and P. Mårtensson, Phys. Rev. B **53**, 13793 (1996).
[10] I. Forbeaux, J.-M. Themlin, and J.-M. Debever, Phys. Rev. B **58**, 16396 (1998).
[11] L. I. Johansson, P. A. Glans, and N. Hellgren, Surf. Sci. **405**, 288 (1998).
[12] I. Forbeaux, J.-M. Themlin, and J.-M. Debever, Surf. Sci. **442**, 9 (1999).
[13] Th. Seyller, K. V. Emtsev, K. Gao, F. Speck, L. Ley, A. Tadich, L. Broekman, J. D. Riley, R. C. G. Leckey, O. Rader, A. Varykhalov, and A. M. Shikin, Surf. Sci. **600**, 3906 (2006).
[14] T. Ohta, A. Bostwick, Th. Seyller, K. Horn, and E. Rotenberg, Science **313**, 951 (2006).
[15] E. Rollings, G.-H. Gweon, S. Y. Zhou, B. S. Mun, J. L. McChesney, B. S. Hussain, A. V. Fedorov, P. N. First, W. A. de Heer, and A. Lanzara, J. Phys. Chem. Solids **67**, 2172 (2006).
[16] A. Bostwick, T. Ohta, Th. Seyller, K. Horn, and E. Rotenberg, Nat. Phys. **3**, 36 (2007).
[17] T. Ohta, A. Bostwick, J. L. McChesney, Th. Seyller, K. Horn, and E. Rotenberg, Phys. Rev. Lett. **98**, 206802 (2007).
[18] A. Bostwick, T. Ohta, J. L. McChesney, K. V. Emtsev, Th. Seyller, K. Horn, and E. Rotenberg, New J. Phys. **9**, 385 (2007).
[19] K. V. Emtsev, Th. Seyller, F. Speck, L. Ley, P. Stojanov, J. D. Riley, and R. G. C. Leckey, Mater. Sci. Forum **556-557**, 525 (2007).
[20] K. V. Emtsev, F. Speck, Th. Seyller, J. D. Riley, and L. Ley, Phys. Rev. B **77**, 155303 (2008).
[21] S. Y. Zhou, G.-H. Gweon, A. V. Fedorov, P. N. First, W. A. de Heer, D.-H. Lee, F. Guinea, A. H. Castro Neto, and A. Lanzara, Nat. Mater. **6**, 770 (2007); **6**, 916 (2007).
[22] J. Hass, R. Feng, T. Li, X. Li, Z. Zong, W. A. de Heer, P. N. First, E. H. Conrad, C. A. Jeffrey, and C. Berger, Appl. Phys. Lett. **89**, 143106 (2006).
[23] J. Hass, F. Varchon, J. E. Millan-Otoya, M. Sprinkle, W. A. de Heer, C. Berger, P. N. First, L. Magaud, and E. H. Conrad, Phys. Rev. Lett. **100**, 125504 (2008).
[24] J. Hass, R. Feng, J. E. Millan-Otoya, X. Li, M. Sprinkle, P. N. First, W. A. de Heer, E. H. Conrad, and C. Berger, Phys. Rev. B **75**, 214109 (2007).
[25] P. Mallet, F. Varchon, C. Naud, L. Magaud, C. Berger, and J.-Y. Veuillen, Phys. Rev. B **76**, 041403(R) (2007).
[26] G. M. Rutter, J. N. Crain, N. P. Guisinger, T. Li, P. N. First, and J. A. Stroscio, Science **317**, 219 (2007).
[27] V. W. Brar, Y. Zhang, Y. Yayon, A. Bostwick, T. Ohta, J. L. McChesney, K. Horn, E. Rotenberg, and M. F. Crommie, Appl. Phys. Lett. **91**, 122102 (2007).
[28] C. Riedl, U. Starke, J. Bernhardt, M. Franke, and K. Heinz, Phys. Rev. B **76**, 245406 (2007).
[29] W. Chen, H. Xu, L. Liu, X. Gao, D. Qi, G. Peng, S. C. Tan, Y. Feng, K. P. Loh, and A. T. S. Wee, Surf. Sci. **596**, 176 (2005).
[30] H. Hibino, H. Kageshima, F. Maeda, M. Nagase, Y. Kobayashi, and H. Yamaguchi, Phys. Rev. B **77**, 075413 (2008).
[31] T. Ohta, F. El Gabaly, A. Bostwick, J. L. McChesney, K. V. Emtsev, A. K. Schmid, Th. Seyller, K. Horn, and E. Rotenberg, New J. Phys. **10**, 023034 (2008).
[32] F. Owman and P. Mårtensson, Surf. Sci. **369**, 126 (1996).
[33] U. Starke, J. Schardt, and M. Franke, Appl. Phys. A: Mater. Sci. Process. **65**, 587 (1997).
[34] U. Starke, M. Franke, J. Bernhardt, J. Schardt, K. Reuter, and K.

Heinz, Mater. Sci. Forum **264-262**, 321 (1998).
[35] K. V. Emtsev, Th. Seyller, and L. Ley (unpublished).
[36] E. Stolyarova, K. T. Rim, S. Ryu, J. Maultzsch, P. Kim, L. E. Brust, T. F. Heinz, M. S. Hybertsen, and G. W. Flynn, Proc. Natl. Acad. Sci. U.S.A. **104**, 9209 (2007).
[37] Y. Hisada, Y. Mitsuoka, S. Mukainakano, H. Suzuki, T. Aoyama, and A. Ichimiya, e-J. Surf. Sci. Nanotechnol. **2**, 8 (2004).
[38] E. McCann, Phys. Rev. B **74**, 161403 (2006).
[39] E. McCann and V. I. Fal'ko, Phys. Rev. Lett. **96**, 086805 (2006).
[40] F. Guinea, Phys. Rev. B **75**, 235433 (2007).
[41] M. Aoki and H. Amawashi, Solid State Commun. **142**, 123 (2007).